Defence Research and Development Canada | Recherche et développement pour la défense Canada

CAN UNCLASSIFIED

DRDC | RDDC technologysciencetechnologie

# Extracting Traditional Anthropometric Measurements from 3-D Body Scans

Chang Shu
Pencheng Xi
National Research Council of Canada

Allan Keefe
DRDC – Toronto Research Centre

Proceedings of the 5th International Digital Human Modeling Symposium

Fraunhofer Institute for Communication, Information Processing and Ergonomics
Bonn, Germany
June 26–28
2017
Pages 138-149

Date of Publication from External Publisher: June 2017



## Defence Research and Development Canada

**External Literature (N)**
DRDC-RDDC-2021-N302
November 2021

CAN UNCLASSIFIED

Canada

**IMPORTANT INFORMATIVE STATEMENTS**

# Extracting Traditional Anthropometric Measurements from 3-D Body Scans

Shu, C.[1], Xi, P.[1], Keefe, A.[2]

[1] National Research Council of Canada
[2] Defence Research and Development Canada

## Abstract

Despite the prevalence of the 3-D body scans, traditional anthropometric measurement is still the dominate form of human body measurement used in the industry. Increasingly, however, traditional measurements are extracted from 3-D body scans. The traditional measurements are simple to use and are well-understood in the industry. In this paper, we introduce a new method for extracting measurements from body scans. Our method is based on accurately locating anthropometric landmarks using a machine learning approach. All of the measurements are defined according to the landmarks. Three types of measurement – linear distance, geodesic distance, and circumference – are considered. We validate the scan-extracted measurements against human measurements using the 2012 Canadian Forces Anthropometric Survey (CFAS) dataset, which consists of 2,200 full body scans.

**Key words:**

anthropometric landmark localization, measurement extraction, non-rigid registration, deep convolutional neural network

# 1 Introduction

Traditional anthropometric measurements are 1-D measurements defined on the surface of human body based on anthropometric landmarks. They are widely used in industry for product design and other ergonomic applications that concern the human body size and shape. Despite the prevalence of the 3-D body scans, traditional anthropometric measurement is still the dominate form of human body measurement used in the industry. This situation is expected to continue in the near future, because current methods and practice are deeply rooted in the 1-D measurement and 3-D anthropometry has not yet provided the necessary tools and methods for designers. Increasingly, however, traditional measurements are extracted from 3-D body scans. The advantage of doing this is that measurements can be taken repeatedly without the human subjects being present, and therefore, unlimited number of measurement can be taken.

A raw 3-D body scan consists of hundreds of thousands of 3-D points. They are unorganized, noisy, and incomplete due to the limitations of the imaging sensor. To extract body measurements from the 3-D scans, the raw scan data have to be processed to extract higher level information. Several methods have been proposed in the literature. NURRE (1997) analyzes the slices that are parallel to the ground and segments the whole body into parts representing limbs, torso, and head. Leong et al. (2007) and LU et al. (2008) study the geometric characteristics of the silhouette and extract features points and curves. The problem of these geometric methods is that they rely on rules to define landmarks and key features. Because of the complex nature of the body shape and the 3-D data, it is difficult to come up with a simple set of rules for this purpose and there are always exceptions, making the algorithm unreliable.

In some 3-D anthropometric surveys, for example, the CAESAR survey (ROBINETTE et al. 2002), anthropometrists marked the anthropometric landmarks on the subjects with photo reflective markers prior to the scanning process. The locations of the landmarks can then be identified on the scans manually or using software. Several authors make use of these landmarks to fit a template mesh to every scan (ALLEN et al., 2003; XI et al. 2007). This method establishes a correspondence or registration among the individual scans, and at the same time, smoothly fills the holes in the scans. The correspondence provides a foundation for statistical shape analysis and other applications including extracting body measurements.

However, landmarking the human subjects is a tedious task and requires expert knowledge of the human anatomy. Several authors proposed methods for locating the landmarks automatically (BEN AZOUZ, 2006; WUHRER, 2010; YAMAZKI, 2013) with moderate success. TSOLI et al. (2014) suggest a data-driven approach to predicting the body measurements by using a markerless registration method and establishing a statistical model between the measurements and the body shapes. However, this method can only predict the measurements that have been taken in the training data.

Since the traditional anthropometric measurements have long been standardized based on the landmarks, any useful system that extracts body measurements has to be able to locate the landmarks robustly. In this paper, we introduce a new method for predicting landmarks based on deep neural networks (LECUN et al. 2015). All of the measurements are defined according to the landmarks. Three types of measurement – linear distance, geodesic distance, and circumference – are considered. We validate the scan-extracted measurements against human measurements using the 2012 Canadian Forces Anthropometric Survey (CFAS) dataset, which consists of 2,200 full body scans.

# 2 Landmark prediction

Anthropometric landmarks are stable corresponding positions on the human body that exist across the population. They are usually located on the human body where bones protrude. Therefore, many of them have visible features on the surface of the human body. This suggests that we can apply a Machine Learning approach to train a computer program using data from manually identified landmarks. In the past, geometric features and explicit models, such as the Markov Random Field model (BEN AZOUZ, 2006), has been used to learn the relationship between the landmarks and their surface features. The recent development in deep neural networks provides a much more flexible and expressive model. A set of tools, called convolutional neural networks (CNN), is particularly effective for solving the image classification problems (KRIZHEVSKY et al. 2012). In this section, we show that they can be adapted for the 3-D meshes and solving the landmarking problem.

## 2.1 Training

In order to use CNN, the data have to be in the form of a 2-D array, such as a color image. Converting the mesh models to images is a crucial step in applying CNN to solve the landmark prediction problem. Although a mesh model is a 3-D object, its surface is a 2-D manifold embedded in 3-space. Therefore, at any given point on the surface, we can extract a local 2-D image. One simple way of reducing the landmark identification problem to an image classification problem is to project the 3D model to an image plane, like taking a photograph of the model, and generate an image using the surface properties of the model. We consider three types of images.

1. Curvature map. At each vertex of the mesh, the two principal surface curvatures are computed and the mean or Gaussian curvature can be evaluated. This is a scalar that can be converted to a color value. We can render the mesh in color by interpolating the vertex colors for every triangle and thus obtain a curvature map. We then project the color model to a plane to generate a color image. Two projection planes were selected, one in front of and another one at the back of the model. Figure 2.1(a) shows an example of the curvature map. The curvature map completely defines the local surface properties of the mesh model.
2. Depth map. With the same front and back image planes chosen as above, we can generate two images in which each pixel value represents the distance from the image plane to the corresponding point on the mesh. These are grey-scale images (Figure 2.1 b), just like the ones obtained with 3-D scanners.
3. Appearance image. We can simulate a camera taking photographs of the 3-D model. An upper front light source is selected and the 3-D model is rendered

into the defined image plane. The shading on the model captured by the virtual camera represents the geometry of the 3-D model. Figure 2.1(c) shows examples of the appearance image.

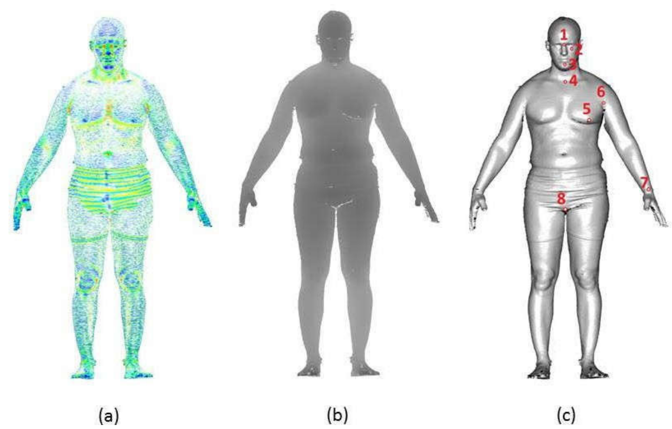


**Fig. 2.1** Images generated from a mesh. (a) curvature map; (b) depth map; (c) appearance image.

## 2.2 Prediction

The most straightforward way of predicting landmarks is to formulate it as a regression problem. This approach trains a regression network that takes an image and outputs the coordinates of the landmarks. FAN and ZHOU (2016) used this approach to localize landmarks on face images and achieved good results. However, for identifying landmarks for the full body, this method cannot deliver sufficient accuracy because the image size that is feasible for CNN is limited. Nonetheless, we can use it as a first approximation of the landmark locations. Based on this approximation, we devise a classification CNN for each landmark.

In our implementation, we use the VGG network (CHATTFIELD et al., 2014), a publicly available network pre-trained with the ImageNet images. It consists of five convolutional layers followed by three fully-connected layers. We customize this network for solving our landmark localization problem. For the regression problem, we remove the last softmax layer and the change the output size of the last fully-connected layer to twice the number of selected landmarks. For computing the loss, we use least square error ($L_2$ norm) for forward and backward loss propagation.

To train a deep classification network, we need both the locations of the true landmarks and the locations for none landmarks. For this purpose, we select nearby pixels, called phantom landmarks, to train the classifier. Images of the phantom landmarks are generated as examples of none-landmarks (Figure 2.2).

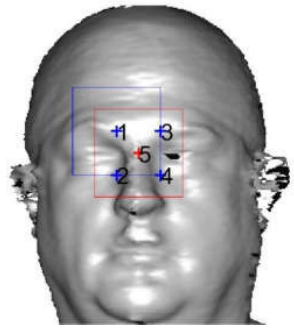


**Fig. 2.2** Phantom landmarks

To modify the VGG network for classification, we first remove the output softmax layer and change the last convolution layer to reflect the size of the output, which is the number of classes for the new classifier. Then we add a new softmax loss layer for the classification of image patches.

When training the network, we keep all of the VGG parameters and weights, only changing the learning rate to ensure convergence. To predict a landmark, we search around the first approximation using a sliding window approach.

We use MatConNet, a MATLAB toolbox for Convolutional Neural Networks (CHATTFIELD et al., 2014) to customize the VGG network. The toolbox provides basic building blocks of a deep CNN, including convolution, pooling, and non-linear activations. It also supports multiple GPUs.

## 2.3 Validation

We use 200 manually landmarked models for training the deep CNN. We also set aside 50 manually landmarked models for validation. The validation dataset is also used for monitoring the learning processes to avoid over-fitting.

The resolution of the image initially generated from the mesh model is 2240x2240. Since VGG requires all images to be 224x224, we scale all the images to this size. The landmark coordinates are projected to the same sized image.

### 2.3.1 Deep regression and classification CNNs

The training of the customized deep regression CNN takes about 40 hours, running 16,000 epochs. The learning rate is set to 0.5*e*-4.

For each landmark, we train a deep CNN classifier. A square image of 80x80 centered at the landmark location is extracted for a positive example. Four other points that are 20 pixels away from the landmark are selected as *phantom landmarks*, to generate negative example images. The collection of both positive and negative example images is used to train the deep classification CNN.

Training the CNN takes about 2.5 hours for completing 12,000 epochs at a learning rate of 0.0002.

### 2.3.2 Prediction results and evaluation

Figure 2.3 illustrates the window-sweeping process for predicting the landmarks. The results are summarized in Table 2.1. We evaluate the maximal absolute difference (MAD) from the predicted landmark to the human marked landmark. We selected 25 landmarks that are important for measurements (Figure 2.4). The mean MAD and the 95% confidence for each landmark are computed. With the exception of the sacrum (landmark 11), the majority of the errors are within 15mm. Note that a landmark like the sacrum, where there is little local surface feature, is difficult to locate even for the human operators. KOUCHI and MOCHIMARU (2011) studied the accuracy of the anthropometrists with a small sample set and reported that the intra-observer errors range from 2mm to 26mm.

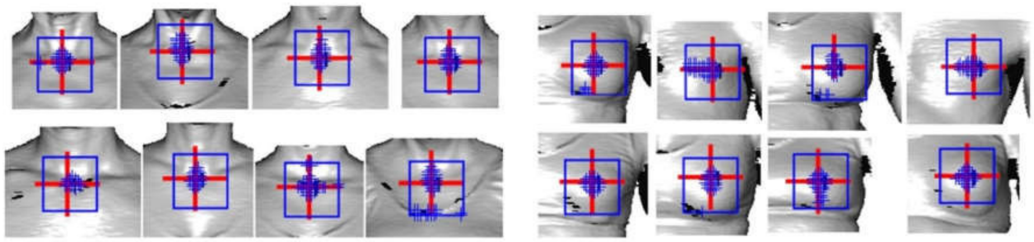

**Fig. 2.3** Examples of the window-sweeping process.

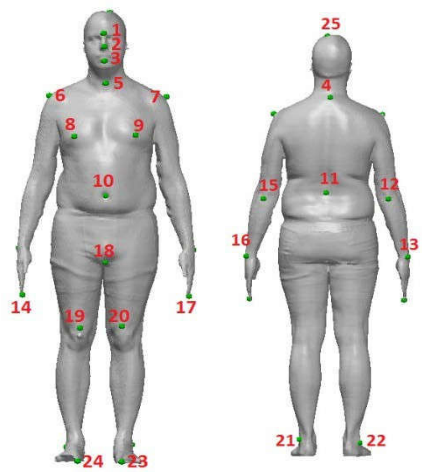


**Fig. 2.4** Landmark index

**Table 2.1** Landmark prediction errors

| Landmark Name | MAD - mean | MAD - std | MAD-mean (95%) | MAD-std (95%) |
|---|---|---|---|---|
| 1 Glabella | 4.25 | 2.13 | 3.98 | 1.88 |
| 2 Most Anterior Point of Nose | 3.99 | 2.02 | 3.71 | 1.67 |
| 3 Mentis | 5.65 | 6.50 | 4.65 | 2.13 |
| 4 Cervicale | 10.60 | 8.77 | 8.93 | 5.39 |
| 5 Anterior Neck | 17.63 | 12.60 | 15.85 | 10.40 |
| 6 Acromion (left) | 9.73 | 3.23 | 9.30 | 2.72 |
| 7 Acromion (right) | 10.31 | 6.37 | 9.24 | 4.62 |
| 8 Bustpoint (left) | 8.61 | 9.33 | 6.83 | 5.62 |
| 9 Bustpoint (right) | 10.50 | 13.66 | 8.01 | 8.94 |
| 10 Omphalion (anterior) | 5.27 | 4.35 | 4.52 | 2.17 |
| 11 Sacrum | 62.61 | 32.80 | 59.22 | 30.40 |
| 12 Olecranon (left) | 13.56 | 17.53 | 10.35 | 10.83 |
| 13 Ulnar Styloid (left) | 14.52 | 17.77 | 11.07 | 8.88 |
| 14 Tip of middle finger (left) | 11.59 | 4.98 | 10.83 | 3.88 |
| 15 Olecranon (right) | 21.70 | 22.68 | 17.50 | 13.15 |
| 16 Ulnar Styloid (right) | 12.18 | 10.28 | 10.36 | 5.45 |
| 17 Tip of middle finger (right) | 13.09 | 22.69 | 9.16 | 4.38 |
| 18 Crotch/Groin | 14.96 | 8.74 | 13.54 | 6.02 |
| 19 Suprapatella (left) | 7.03 | 3.79 | 6.49 | 3.10 |
| 20 Suprapatella (right) | 20.50 | 11.22 | 18.73 | 8.31 |
| 21 Lateral Malleolus (right) | 10.74 | 7.35 | 9.62 | 4.74 |
| 22 Lateral Malleolus (left) | 10.54 | 9.84 | 8.93 | 5.53 |
| 23 Left Most Anterior Metatarsal | 7.63 | 10.11 | 5.34 | 2.68 |
| 24 Right Most Anterior Metatarsal | 6.91 | 6.73 | 5.54 | 3.51 |
| 25 Vertex | 22.44 | 10.19 | 21.24 | 9.10 |

# 3 Measurement Extraction

With the predicted the landmarks, we fit a template mesh to every scan. Dimensional measurements are extracted from the fitted models. This way, we can avoid the noisy surface and holes in the raw scans, which can cause errors in computing the measurements.

From a computational perspective, there are three types of measurements: linear distance, geodesic distance, and circumference, all related to the landmarks. The linear distance is the simplest to implement; it is just the Euclidean distance between two landmark points. Examples of linear distance are Cervicale Height, Ankle Height, and Chest Height.

The geodesic distance is the shortest path length from one point to another along the surface. It is equivalent to flatten the surface locally and connecting the two points with a straight line. This geometric procedure closely approximates the tape measure operation performed by a human operator. Examples of geodesic distance include the waist back length and the sleeve outstream.

Circumferences are computed by intersecting a plane with the model and calculating the length of the intersecting curve. Examples of circumference are Waist, Ankle, and Neck circumferences. Note that in general a cutting plane may result in multiple loops and the correct loop has to be selected. This can be done by pre-segmenting the body into parts and the cutting is only performed on the correct part. For some measurements, the cutting curve is not convex and is not the same as the tape measure. This can be compensated by computing the convex hull of the cutting curve. The convex hull of a set of points in the smallest convex polygon that encloses the point set.

## 3.1 Validation

In general, it is difficult to evaluate the accuracy of the extracted dimensions simply because there is no ground truth for these dimensions. The shape and size of a human are constantly changing due to breathing and posture variation. Different operators have slightly different interpretations of a definition of a measurement and therefore will obtain different results for the same person.

In traditional anthropometric surveys, human operators are often tested for consistency. A measurement is taken multiple times on a subject by the same operator during a day. The Mean Absolute Difference (MAD) is computed to gauge the operator’s reliability (GORDON et al., 1989).

ROBINETTE and DAANEN (2006) studied the consistency of scan-extracted measurements by scanning a subject multiple times and extracting the measurements by software. They reported that the consistency of the scan-extracted measurements is comparable to that of expert anthropometrists.

As the goal of extracting traditional anthropometric measurements from 3-D models is to simulate a human operator performing the measurements, one reasonable validation is to compare with manual measurements for the likewise measurements.

BRADTMILLER and GROSS (1999) and PAQUETTE et al. (2000) evaluated proprietary software against human anthropometrists.

**Table 3.1** Comparison with manual measurements (error in mm)

| Measurement Names | Mean MAD | MAD Std |
|---|---|---|
| 'Acromion-Radiale Length' | 20.1 | 17.6 |
| 'Ankle Circumference' | 25.5 | 10.0 |
| 'Axilla Height' | 21.0 | 13.4 |
| 'Bitragion Breadth' | 7.9 | 3.5 |
| 'Bustpoint/Thelion-Bustpoint/Thelion Breadth' | 14.5 | 20.3 |
| 'Buttock Depth' | 26.9 | 10.9 |
| 'Buttock Height' | 24.6 | 15.8 |
| 'Calf Circumference' | 8.0 | 6.9 |
| 'Calf Height' | 15.3 | 13.4 |
| 'Cervicale Height' | 27.9 | 20.5 |
| 'Chest Depth' | 6.5 | 5.1 |
| 'Chest Height' | 15.7 | 13.2 |
| 'Elbow Circumference' | 15.2 | 9.7 |
| 'Head Length' | 6.5 | 4.6 |
| 'Lateral Malleolus Height' | 12.8 | 9.1 |
| 'Neck Circumference, Base' | 22.8 | 24.2 |
| 'Radiale-Stylion Length' | 21.1 | 20.1 |
| 'Stature' | 21.5 | 8.2 |
| 'Suprasternale Height' | 14.7 | 10.8 |
| 'Tenth Rib Height' | 35.0 | 20.6 |
| 'Thigh Circumference' | 38.1 | 41.8 |
| 'Trochanterion Height' | 19.5 | 12.7 |
| 'Waist Back Length (Omphalion)' | 32.3 | 26.0 |
| 'Waist Circumference (Omphalion)' | 38.7 | 63.3 |
| 'Waist Depth' | 11.2 | 9.0 |
| 'Waist Front Length (Omphalion)' | 39.1 | 39.4 |
| 'Waist Height (Omphalion)' | 24.7 | 25.9 |
| 'Sleeve Outseam' | 34.1 | 28.1 |
| 'Knee Circumference' | 21.4 | 14.3 |
| 'Neck-Bustpoint/Thelion Length' | 16.5 | 24.9 |
| 'Shoulder Length' | 10.0 | 6.4 |

We conduct a preliminary test that compares the machine extracted results to those obtained by traditional anthropometry using 30 subjects. Table 2 shows the statistics of these comparisons. Note that the MADs are significantly higher than the ISO 20685 (2010) specified allowable errors, which are less than 1 cm for all measurements. This shows that our measurement extraction process has significant differences with the human operators in terms of interpreting the definitions of the measurements, given that we have relative accurate prediction of the landmarks. We have also analyzed the positive / negative bias of the results and found that most computed measurements are larger than the manual measurements. This may be due to the fact that the human operators apply a tension to the measuring tape. The results can be improved by calibrating the machine computed dimensions with those obtained by the anthropometrists. Further investigation is necessary using more data.

# 4 Conclusions

Physical measurement extraction allows measurements to be taken from the scans at any time and an extended range of measurements to include those that have not been considered at the time of the survey. It is also possible to perform measurements more consistently, as demonstrated by ROBINETTE and DAANEN (2006). The key issue is to find the landmarks accurately. In this paper, we have shown that the deep convolutional neural network can be used effectively to solve this problem. Once we have a reasonable set of landmarks, we can fit a template mesh to each scan, and from there, we can compute the measurements using standard geometric algorithms.

Comparing to the human measurements, certain scan-extracted measurements are more accurate. For example, the calf circumference, defined as the maximal circumference of the lower leg, can be computed precisely by a search algorithm, while human operators can only estimate.

It is necessary to note that the machine measurements will always be different from the manual measurements, because many different factors are involved in the two processes. However, as we train the computer to identify landmarks like the human exports, we will be more confident to extract reliable body dimensions from the scans automatically.

# List of references

Allen, B.; Curless, B.; Popovic, Z.: The space of human body shapes: reconstruction and parameterization from range scans, ACM Transactions on Graphics, 22(3): 587-594, 2003.

Ben Azouz, Z.; Shu, C.; Mantel, A.: Automatic Locating of Anthropometric Landmarks on 3D Human Models, Third International Symposium on 3D Data Processing, Visualization and Transmission (3DPVT 2006). Chapel Hill, North Carolina, USA. June 13-16, 2006.

Bradtmiller, B.; Gross, M.: 3D Whole Body Scans: Measurement Extraction Software Validation, SAE Technical Paper 1999-01-1892, 1999.

Chatfield, K.; Simonyan, K.; Vedaldi, A.; Zisserman, A.: Return of the devil in the details: Delving deep into convolutional nets. In British Machine Vision Conference, 2014.

Fan, H.; Zhou, E.: Approaching human level facial landmark localization by deep learning, Image and Vision Computing, 47:27-35, 2016. 300W, the First Automatic Facial Landmark Detection in-the-wild Challenge.

Gordon, C. C.; Bradmiller, B.; Clausen, C. E.; Churchill, T.; McConville, J. T.; Tebbetts, I.; Walker, R. A.: 1987-1988 Anthropometric survey of US Army personnel. Methods and summary statistics. Natick/TR-89-044. US Army Natick Research Development and Engineering Center, Natic, MA.; 1989.

ISO 20685:2010, 3-D scanning methologies for internationally compatible anthropometric databases.

Kouchi, M.; Mochimaru, M.: Errors in landmarking and the evaluation of the accuracy of traditional and 3D anthropometry, Applied Ergonomics, 42:518-527, 2011.

Krizhevsky, A.; Sutskever, I.; Hinton, G. E.: ImageNet classification with deep convolutional neural networks, Advances in Neural Information Processing Systems (NIPS), 2012.

LeCun, Y.; Bengio, Y.; Hinton, G.: Deep learning, Nature, 2015.

Leong, I.; Fang, J.; Tsai, M.: Automatic body feature extraction from a marker-less scanned human body, Computer-Aided Design, 39:568-582, 2007.

Lu, J.; Wang, M.: Automated anthropometric data collection using 3D whole body scanners, Expert Systems with Applications, 35:407-414, 2008.

Nurre, J. H.: Locating landmarks on human body scan data, International Conference on Recent Advances in 3-D digital imaging and modeling, pp. 289-295, 1997.

Paquette, S.; Brantley, J. D.; Corner, B.; Li, P.; Oliver, T.: Automated extraction of anthropometric data from 3D images, Proceedings of the IEA 2000 / HFES 2000 Congress.

Robinette, K.; Daanen, H.: Precision of the CAESAR scan-extracted measurements, Applied Ergonomics, 37(3):259-265, 2006.

Robinette, K.; Blackwell, S.; Daanen, H.; Fleming, S.; Boehmer, M.; Brill, T.; Hoeferlin, D.; Burnsides, D.: Civilian American and European surface anthropometry resource (CAESAR), Final Report, Summary, vol. 1. AFRL-HE-WP-2002-0169, 2002.

Aggeliki, T.; Loper, M.; Black, M. J.: Model-based Anthropometry: Predicting Measurements from 3D Human Scans in Multiple Poses, IEEE Winter Conference on Applications of Computer Vision (WACV), 2014.

Wuhrer, S.; Azouz, Z. B.; Shu, C.: Posture invariant surface description and feature extraction. In Computer Vision and Pattern Recognition (CVPR), pages 374–381, June 2010.

Xi, P.; Lee, W.-S.; Shu, C.: Analysis of segmented human body scans. In Proceedings of Graphics Interface 2007, GI'07, pages 19–26, New York, NY, USA, 2007.

Yamazaki, S.; Kouchi, M.; Mochimaru, M.: Markerless landmark localization on body shape scans by non-rigid model fitting, 2nd International Digital Human Modeling Symposium, 2013.

**DOCUMENT CONTROL DATA**

*Security markings for the title, authors, abstract and keywords must be entered when the document is sensitive

| | |
|---|---|
| 1. ORIGINATOR (Name and address of the organization preparing the document. A DRDC Centre sponsoring a contractor's report, or tasking agency, is entered in Section 8.)<br><br>Federal Institute of Occupational Safety and Health<br>Postbox 17 02 02<br>D-44061 Dortmund, Germany<br><br>https://www.baua.de/ | 2a. SECURITY MARKING (Overall security marking of the document including special supplemental markings if applicable.)<br><br>CAN UNCLASSIFIED<br><br>2b. CONTROLLED GOODS<br><br>NON-CONTROLLED GOODS<br>DMC A |

3. TITLE (The document title and sub-title as indicated on the title page.)

Extracting Traditional Anthropometric Measurements from 3-D Body Scans

4. AUTHORS (Last name, followed by initials – ranks, titles, etc., not to be used)

Shu, C.; Xi, P.; Keefe, A.

| 5. DATE OF PUBLICATION (Month and year of publication of document.) | 6a. NO. OF PAGES (Total pages, including Annexes, excluding DCD, covering and verso pages.) | 6b. NO. OF REFS (Total references cited.) |
|---|---|---|
| June 2017 | 12 | 19 |

7. DOCUMENT CATEGORY (e.g., Scientific Report, Contract Report, Scientific Letter.)

External Literature (N)

8. SPONSORING CENTRE (The name and address of the department project office or laboratory sponsoring the research and development.)

DRDC – Toronto Research Centre
Defence Research and Development Canada
1133 Sheppard Avenue West
Toronto, Ontario M3K 2C9
Canada

| 9a. PROJECT OR GRANT NO. (If appropriate, the applicable research and development project or grant number under which the document was written. Please specify whether project or grant.) | 9b. CONTRACT NO. (If appropriate, the applicable number under which the document was written.) |
|---|---|
| | |

| 10a. DRDC PUBLICATION NUMBER (The official document number by which the document is identified by the originating activity. This number must be unique to this document.) | 10b. OTHER DOCUMENT NO(s). (Any other numbers which may be assigned this document either by the originator or by the sponsor.) |
|---|---|
| DRDC-RDDC-2021-N302 | |

11a. FUTURE DISTRIBUTION WITHIN CANADA (Approval for further dissemination of the document. Security classification must also be considered.)

Public release

11b. FUTURE DISTRIBUTION OUTSIDE CANADA (Approval for further dissemination of the document. Security classification must also be considered.)

12. KEYWORDS, DESCRIPTORS or IDENTIFIERS (Use semi-colon as a delimiter.)

Digital Human Modeling; Anthropometry; Landmarking; Measurement; Extraction; Machine Learning

13. ABSTRACT/RÉSUMÉ (When available in the document, the French version of the abstract must be included here.)

Despite the prevalence of the 3-D body scans, traditional anthropometric measurement is still the dominate form of human body measurement used in the industry. Increasingly, however, traditional measurements are extracted from 3-D body scans. The traditional measurements are simple to use and are well-understood in the industry. In this paper, we introduce a new method for extracting measurements from body scans. Our method is based on accurately locating anthropometric landmarks using a machine learning approach. All of the measurements are defined according to the landmarks. Three types of measurement– linear distance, geodesic distance, and circumference – are considered. We validate the scan-extracted measurements against human measurements using the 2012 Canadian Forces Anthropometric Survey (CFAS) dataset, which consists of 2,200 full body scans.